An efficient wavefield inversion for isotropic elastic media

Chao Song, Tariq Alkhalifah*, Guanchao Wang† and Qingjie Yang ‡*
**King Abdullah University of Science and Technology.*
†*China University of Petroleum-Beijing.*
‡*1. Department of Earth Sciences, Memorial University of Newfoundland, 2. State Key Laboratory of Geodesy and Earths Dynamics, Institute of Geodesy and Geophysics*

SUMMARY

Full-waveform inversion (FWI) is a highly non-linear optimization problem which aims at retrieving high-resolution models of the subsurface parameters. Elastic FWI (EFWI) should provide a better representation to the elastic nature of the subsurface than the simple acoustic assumption. However, including elastic parameters in the EFWI requires higher the computational cost and storage memory not to mention the added complexity of dealing with multi parameters and higher nonlinearity in the inversion. To mitigate these problems, we propose an efficient wavefield inversion (EWI) for elastic media. By inverting for a background model wavefield that partially fits the data and the wave equation for a modified source, we are able to extend the search space at a reduced cost. It also saves the storage memory by avoiding storing the background wavefields. We formulate the P- and S-wave velocity perturbations into a linear inversion system to reduce the tradeoff in the multi-parameter waveform inversion. Applications on synthetic data generated from a modified Overthrust model and a modified Marmousi model show the effectiveness of the proposed method.

INTRODUCTION

Full-waveform inversion (FWI) was initially suggested to mainly handle media (Tarantola, 1984). After decades of developments and considering our limitations on acquisition and computational resources, the acoustic assumption has dominated the FWI seen (Virieux and Operto, 2009). In addition, the conventional objective function based on the l_2 norm least-squares measurement is not convex. As a result, FWI suffers from the cycle-skipping problem when reasonable initial models are unavailable and low-frequency components of the data are missing. To make FWI more practical and effective, new optimization problems were developed to mitigate the cycle-skipping (Leeuwen and Herrmann, 2013, 2015). Unlike conventional FWI in which we simulate the predicted data which strictly follows the wave equation, wavefield reconstruction inversion (WRI) relaxes the wave equation accuracy and uses it as a regularization term in inverting for the wavefield. WRI uses the wavefield to update the velocity in each iteration, and thus, it requires many relatively expensive iterations. A new formulation referred to as efficient wavefield inversion (EWI) improves the computational efficiency by introducing a modified source that absorbs the velocity perturbations and relaxes the requirement for a frequent velocity update (Alkhalifah, 2019). EWI calculates parameter perturbations using a direct division (deconvolution), and it has been proved effective and efficient both in acoustic isotropic and VTI media (Alkhalifah and Song, 2019a,b). In elastic FWI (EFWI), we use multicomponent data and try to extract more information of the subsurface. As a result, the nonlinearity of EFWI increases because of the additional NULL space. To mitigate the cycle-skipping problem in EFWI, many new approaches were proposed. Guo and Alkhalifah (2017) and Li et al. (2017) used a nonlinear objective function to invert for the background velocity and the reflectivity, simultaneously, without and with considering the density, respectively. Zhang et al. (2018) proposed a normalized nonzero-lag crosscorrelation objective function to mitigate the cycle skipping.

In this abstract, we linearise the EFWI objective function by dividing the general optimization problem into alternating sub problems. Besides efficiency and memory saving advantages which hold for acoustic EWI, it can also reduce the tradeoff between P- and S-wave velocities. Applications on synthetic data generated from the modified elastic Overthrust and Marmousi models show that the proposed approach can yield reasonable inverted medium parameter models in an efficient matter.

THEORY

In 2D isotropic constant density elastic media, the components of the wavefield in the frequency domain satisfy the following relations (Min et al., 2000; Choi et al., 2008):

$$\begin{aligned} -\rho\omega^2 u &= (\lambda+2\mu)\frac{\partial^2 u}{\partial x^2}+\mu\frac{\partial^2 u}{\partial z^2}+(\lambda+\mu)\frac{\partial^2 v}{\partial x\partial z},\\ -\rho\omega^2 v &= (\lambda+2\mu)\frac{\partial^2 v}{\partial z^2}+\mu\frac{\partial^2 v}{\partial x^2}+(\lambda+\mu)\frac{\partial^2 u}{\partial x\partial z}, \end{aligned} \quad (1)$$

where u and v denote the horizontal and vertical displacements. respectively. ω is the angular frequency, and ρ represents the density. λ and μ are Lamé constants. As P- and S-wave velocities v_p, v_s, Lamé constants and density have the following relations: $v_p=\sqrt{\frac{\lambda+2\mu}{\rho}}, v_s=\sqrt{\frac{\lambda}{\rho}}$. Equation 1 can be re-written as:

$$\begin{aligned} \omega^2 u+v_p^2\frac{\partial^2 u}{\partial x^2}+v_s^2\frac{\partial^2 u}{\partial z^2}+(v_p^2-v_s^2)\frac{\partial^2 v}{\partial x\partial z} &= f_x,\\ \omega^2 v+v_p^2\frac{\partial^2 v}{\partial z^2}+v_s^2\frac{\partial^2 v}{\partial x^2}+(v_p^2-v_s^2)\frac{\partial^2 u}{\partial x\partial z} &= f_z, \end{aligned} \quad (2)$$

where, f_x and f_z are the source functions. The frequency domain elastic wave equations can be expressed in a compact form as:

$$\mathbf{S}(\mathbf{x},\omega)\hat{u}(\mathbf{x},\omega)=\hat{f}(\mathbf{x_s},\omega), \quad (3)$$

where, $\mathbf{S}(\mathbf{x},\omega)$ is the impedance matrix, which is also referred to as the modelling operator. $\hat{u}(\mathbf{x},\omega) = [u\ v]^T$ represents the wavefield vector, and $\hat{f}(\mathbf{x},\omega) = [f_x\ f_z]^T$ represents the source vector. $\mathbf{x}$ and $\mathbf{x_s}$ represent the Cartesian coordinate spatial dimensions and source locations. The wavefield $\hat{u}$ is calculated using the elastic wave equation formulated by elastic medium parameters. The conventional l_2 norm objective function is highly non-linear, which imposes a big challenge in FWI. Beside the nonlinearity issue, FWI requires a large amount of computational cost and storage memory. In order to solve these problems, we use EWI to perform the multi-parameter inversion in isotropic elastic media. The objective function of EWI is given by:

$$E(\hat{u_i},\hat{f_{ei}}) = min\frac{1}{2}\sum_i \|d_i - C\hat{u_i}\|_2^2 + \frac{\alpha}{2}\left\|\mathbf{S_0}(\mathbf{x},\omega)\hat{u_i} - \hat{f_{ei}}\right\|_2^2, \tag{4}$$

where, i is the source index, and α acts as a weighting factor on the background wave equation. At the beginning of the inversion process, we start with a background elastic modelling operator $\mathbf{S_0}$ corresponding to the background medium parameters: v_{p0}, v_{s0}. The data vector $d = [d_x\ d_z]^T$ is made up of x and z components, which are extracted from the horizontal and vertical wavefields using a mapping operator C. $\hat{f_e}(\mathbf{x},\omega) = [f_{ex}\ f_{ez}]^T$ represents the modified source vector, which contains the secondary sources (parameter perturbations). As the wavefield $\hat{u}$ is an independent parameter with respect to the new formulation, we calculate the wavefield vector $\hat{u}$ by solving the following linear equation:

$$\begin{pmatrix}\alpha\mathbf{S_0}\\ C\end{pmatrix}\hat{u_i} = \begin{pmatrix}\varepsilon\hat{f_{ei}}\\ d_i\end{pmatrix}. \tag{5}$$

Equation 5 is solved by a least squares optimization, and we obtain reconstructed wavefields of horizontal and vertical displacements, consequently. Same as the wavefield $\hat{u}$, the modified source function $\hat{f_e}$ is also a linear parameter with respect to the EWI objective function in equation 4. So we minimize E by solving $\nabla_{\hat{f_e}} E = 0$. The modified source function which satisfies the wave equation using the background operator is calculated as:

$$\hat{f_e} = \mathbf{S_0}\hat{u}. \tag{6}$$

We use a finite-difference approximation to represent the elastic wave operator in equation 5 and 6, and the matrix form is expressed as:

$$\begin{bmatrix}\omega^2 D_m + (\alpha D_{xx} + \beta D_{zz}) & (\alpha-\beta)D_{xz}\\ (\alpha-\beta)D_{xz} & \omega^2 D_m + (\beta D_{xx} + \alpha D_{zz})\end{bmatrix}\begin{bmatrix}u\\ v\end{bmatrix} = \begin{bmatrix}f_x\\ f_z\end{bmatrix} \tag{7}$$

where $\alpha = v_p^2$ and $\beta = v_s^2$; D_{zz}, D_{xz}, and D_{xx} denote the finite-difference operators for spatial derivatives; D_m is the mass acceleration operator. We perturb α and β as $\delta\alpha$ and $\delta\beta$, and define the background squared P- and S-wave velocities as α_0 and β_0.

$$\alpha = \alpha_0 + \delta\alpha\ ,\ \beta = \beta_0 + \delta\beta; \tag{8}$$

With α_0 and β_0, equation 6 can be expressed as:

$$\begin{bmatrix}\omega^2 D_m + (\alpha_0 D_{xx} + \beta_0 D_{zz}) & (\alpha_0-\beta_0)D_{xz}\\ (\alpha_0-\beta_0)D_{xz} & \omega^2 D_m + (\beta D_{xx} + \alpha_0 D_{zz})\end{bmatrix}\begin{bmatrix}u\\ v\end{bmatrix} = \begin{bmatrix}f_{ex}\\ f_{ez}\end{bmatrix} \tag{9}$$

Subtracting equation 7 from equation 9, we get relations between squared P- and S-wave velocity perturbations and the modified source functions, which are:

$$\begin{aligned}(\delta\alpha D_{xx} + \delta\beta D_{zz})u + (\delta\alpha D_{xz} - \delta\beta D_{xz})v &= f_x - f_{ex},\\ (\delta\beta D_{xx} + \delta\alpha D_{zz})v + (\delta\alpha D_{xz} - \delta\beta D_{xz})u &= f_z - f_{ez},\end{aligned} \tag{10}$$

Consequently, for each grid point, we can calculate $\delta\alpha$ and $\delta\beta$ by solving a 2 by 2 matrix given by:

$$\begin{bmatrix}D_{xx}u + D_{xz}v & D_{zz}u - D_{xz}v\\ D_{xz}u + D_{zz}v & D_{xx}v - D_{xz}u\end{bmatrix}\begin{bmatrix}\delta\alpha\\ \delta\beta\end{bmatrix} = \begin{bmatrix}f_x - f_{ex}\\ f_z - f_{ez}\end{bmatrix} \tag{11}$$

However, this is costly for large models, as we need to solve a lot of linear inversions granted they correspond to small-size matrices. For a linear inversion system $Ax = b$, we often use a damped least squares optimization using $x = \left[A^TA + \lambda I\right]^{-1}A^Tb$. In this case, λ is a weighting factor, which plays an important role to stabilize the solution. One inversion strategy requires to solve a large number of small linear inversion systems of $Ax = b$ for each grid point independently, but we cannot afford to find a suitable λ for each solution. To solve this problem, we combine the inversion into a large single linear tridiagonal inverse problem expressed as:

$$\begin{bmatrix}a_1 & & & b_1 & & \\ & \dots & & & \dots & \\ & & a_N & & & b_N\\ c_1 & & & d_1 & & \\ & \dots & & & \dots & \\ & & c_N & & & d_N\end{bmatrix}\begin{bmatrix}\delta\alpha_1\\ \dots\\ \delta\alpha_N\\ \delta\beta_1\\ \dots\\ \delta\beta_N\end{bmatrix} = \begin{bmatrix}(f_x - f_{ex1})\\ \dots\\ (f_{xN} - f_{exN})\\ (f_{z1} - f_{ez1})\\ \dots\\ (f_{zN} - f_{ezN})\end{bmatrix} \tag{12}$$

where, $a = D_{xx}u + D_{xz}v$, $b = D_{zz}u - D_{xz}v$, $c = D_{xz}u + D_{zz}v$, and $d = D_{xx}v - D_{xz}u$. This linear inversion system can be represented: $Ax = b$. The size of matrix A is $2N$ by $2N$, where N is the number of the model grid points. The vector x consists of P- and S-wave velocity perturbations of the whole model, and the vector b consists of the difference between the original source f and the modified source $\hat{f_e}$. Instead of directly using the damped least squares solution, we use an iterative refinement method to reduce the residual errors (Aghamiry et al., 2019). This method iteratively updates the right-hand side of $Ax = b$. In the first iteration, the solution satisfies:

$$x_1 = \arg\min_x \|Ax - b\|_2^2 = A^{-g}b, \tag{13}$$

where $A^{-g} = \left[A^TA + \lambda I\right]^{-1}A^T$ represents the generalised inverse of matrix A. The right-hand side b_1 corresponding to x_1 is given by: $b_1 = Ax_1$. The residual error is $\delta b_1 = b - b_1$. In order to correct the residual δb_1, we can easily evaluate the perturbation $\delta x = x - x_1$ through

$$\delta x_1 = \arg\min_x \|A\delta x - \delta b_1\|_2^2, \tag{14}$$

As a result, we can update the model: $x_2 = x_1 + A^{-g}\delta b_1 = A^{-g}b + A^{-g}(b - Ax_1)$. To summarize, if we repeat this procedure k times, the final solution is evaluated through:

$$x_k = A^{-g}b + \sum_{i=1}^{k-1}A^{-g}(b - Ax_i) = A^{-g}[b + \sum_{i=1}^{k-1}(b - Ax_i)], \tag{15}$$

EXAMPLES

The key point of EWI is to invert for an accurate, or close enough, wavefield using the background operator $\mathbf{S_0}(\mathbf{x}, \omega)$. We firstly consider a homogeneous model with true P- and S-wave velocities being 2.2 km/s and 1.2 km/s, respectively. We use a longitudinal wave source located in the middle of the model, and receivers at all boundaries. With the background P- and S-wave velocities being lower than the actual ones, at 2.0 km/s and 1.0 km/s, and with $\varepsilon = 10e^{-15}$, we use two inner iterations between equations 5 and 6 to invert for the wavefields of horizontal and vertical displacements. We compare the true wavefields with the background and reconstructed wavefields of horizontal and vertical displacements for 5 Hz in Figures 1 and 2, respectively. We observe that there are clear mismatches between the true and background wavefields in both components, while the reconstructed wavefields are close to the true wavefields. Alternatively, these reconstructed wavefields can be used to invert for the modified source function $\hat{f}_e$ including the P- and S-wave velocity perturbations.

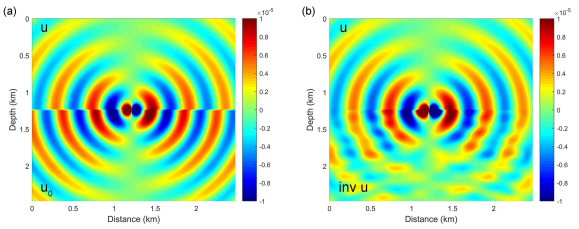

Figure 1: The true (top a and b), background (bottom a) and reconstructed (bottom b) wavefields of horizontal displacements.

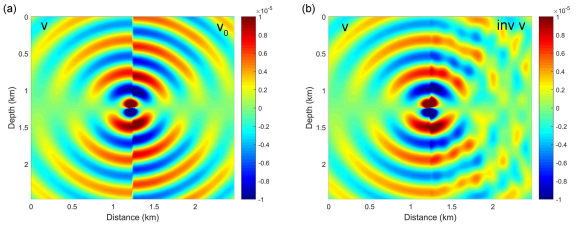

Figure 2: The true (left a and b), background (right a) and reconstructed (right b) wavefields of vertical displacements.

We next apply the proposed method on a modified Overthrust model. The true P- and S-wave velocities are shown in Figure 3. We use 20 sources uniformly distributed on the surface, and all the grid points on the surface act as receivers. The initial P- and S-wave velocities are 1D linearly increasing with depth models as shown in Figure 4.

We perform EWI from 3 Hz to 10 Hz with a sampling interval of 0.5 Hz in the frequency domain, and in each frequency we use two inner iterations and 10 outer iterations. The ε we use here is $10e^{-15}$. The inversion results are shown in Figure 5. Using the same inversion setup and strategy, we perform FWI on the same model. It is obvious that EWI recovers true models reasonably well. While the optimization using FWI apparently falls into a local minimum, the inverted P- and S-wave velocities in the deep part are not well recovered.

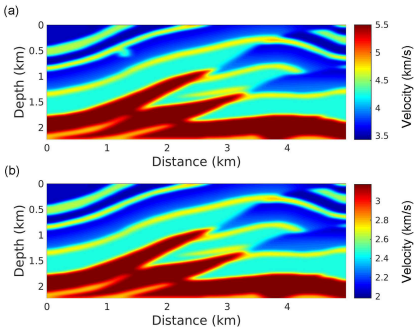

Figure 3: The true Overthrust P-wave velocity model (a), and S-wave velocity model (b).

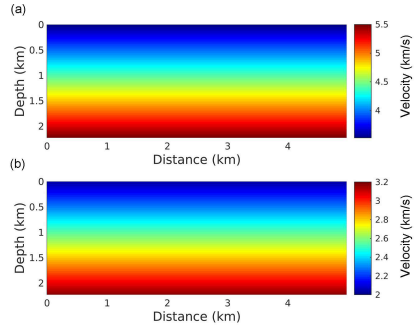

Figure 4: The initial Overthrust P-wave velocity model (a), and S-wave velocity model (b).

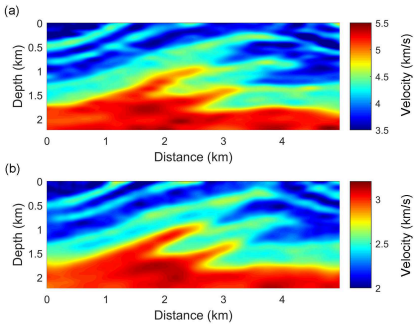

Figure 5: The inverted Overthrust P-wave velocity model (a), and S-wave velocity model (b) using EWI.

We further apply the elastic EWI on a modified elastic Marmousi model, where the true P- and S-wave velocity models include differences beyond a fixed Poisson's ratio as the red arrows point out, which are shown in Figures 7a and 7b. The initial P- and S-wave velocity models are linearly increasing with depth, which are shown in Figures 8a and 8b. There are 76 sources with 125 m spacing interval and 377 receivers evenly distributed on the surface. We perform EWI and FWI in this example using the same inversion setup as the previous one, and the inversion results are shown in Figures 9 and 10. We observe that EWI can almost recover all the structural fea-

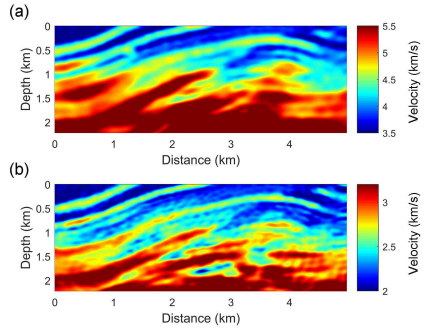

Figure 6: The inverted Overthrust P-wave velocity model (a), and S-wave velocity model (b) using FWI.

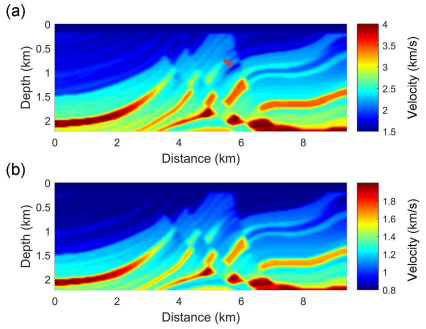

Figure 7: The true Marmousi P-wave velocity model (a), and S-wave velocity model (b).

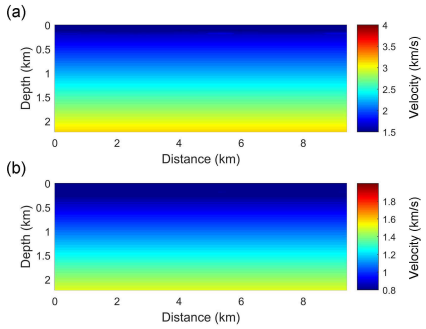

Figure 8: The initial Marmousi P-wave velocity model (a), and S-wave velocity model (b).

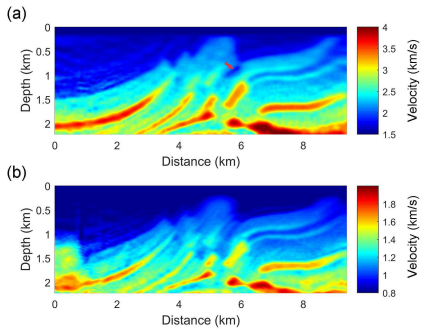

Figure 9: The inverted Marmousi P-wave velocity model (a), and S-wave velocity model (b) using EWI.

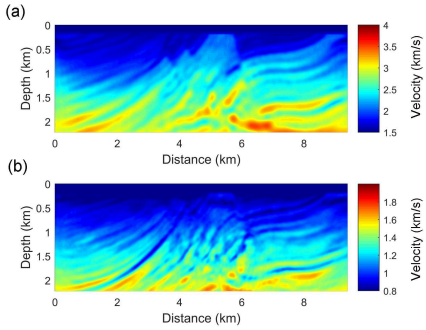

Figure 10: The inverted Marmousi P-wave velocity model (a), and S-wave velocity model (b) using FWI.

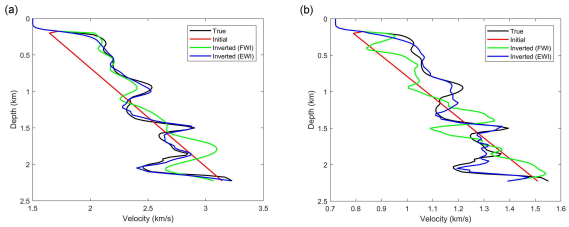

Figure 11: The P-wave velocity profile (a), and S-wave velocity profile (b) at 5 km.

tures in the P- and S-wave velocity models, while FWI fails to deliver good inversion results due to the cycle-skipping issue. This is more obvious in the P- and S-wave velocity profiles at 5 km shown in Figures 11a and 11b. Clearly, the inverted P- ans S-wave velocities using the proposed method fit the true models better than the inverted results of the conventional EFWI.

CONCLUSIONS

We apply an efficient wavefield inversion to isotropic elastic media. By using a modified source function to accommodate the velocity perturbations, we divide the nonlinear optimization problem into several linear sub-problems. After optimizing the reconstructed wavefields and modified sources, we formulate a linear inversion problem for the P- and S- waves velocity perturbations by an iterative refined method. As a result, P- and S-wave velocities can be inverted simultaneously with high accuracy. We have shown the effectiveness of the approach on synthetic data and we plan to show results from field data as part of the presentation.

ACKNOWLEDGMENTS

We thank KAUST for sponsoring this research. We thank our SWAG colleagues for their helpful suggestions.

REFERENCES

Aghamiry, H. S., A. Gholami, and S. Operto, 2019, Improving full-waveform inversion by wavefield reconstruction with the alternating direction method of multipliers: Geophysics, **84**, R139–R162.

Alkhalifah, T., 2019, Linear wavefield optimization using a modified source: Communications in computational physics, accepted.

Alkhalifah, T., and C. Song, 2019a, An efficient wavefield inversion: 81th EAGE Conference and Exhibition.

———, 2019b, An efficient wavefield inversion for transversely isotropic media with a vertical symmetry axis: 81th EAGE Conference and Exhibition.

Choi, Y., D.-J. Min, and C. Shin, 2008, Frequency-domain elastic full waveform inversion using the new pseudo-hessian matrix: Experience of elastic marmousi-2 synthetic data: Bulletin of the Seismological Society of America, **98**, 2402–2415.

Guo, Q., and T. Alkhalifah, 2017, Elastic reflection-based waveform inversion with a nonlinear approach: Geophysics, **82**, R309–R321.

Leeuwen, T. V., and F. Herrmann, 2013, Mitigating local minima in full-waveform inversion by expanding the search space: Geophysical Journal International, **195**, 661–667.

———, 2015, A penalty method for pde-constrained optimization in inverse problems: Inverse Problems, **32**, 015007.

Li, Y., Z. Li, T. Alkhalifah, and Q. Guo, 2017, Elastic reflection waveform inversion with variable density, *in* SEG Technical Program Expanded Abstracts 2017: Society of Exploration Geophysicists, 1545–1550.

Min, D.-J., C. Shin, B.-D. Kwon, and S. Chung, 2000, Improved frequency-domain elastic wave modeling using weighted-averaging difference operatorsfrequency-domain elastic modeling: Geophysics, **65**, 884–895.

Tarantola, A., 1984, Inversion of seismic reflection data in the acoustic approximation: Geophysics, **49**, 1259–1266.

Virieux, J., and S. Operto, 2009, An overview of full-waveform inversion in exploration geophysics: Geophysics, **74**, WCC1–WCC26.

Zhang, Z., T. Alkhalifah, Z. Wu, Y. Liu, B. He, and J. Oh, 2018, Normalized nonzero-lag crosscorrelation elastic full-waveform inversion: Geophysics, **84**, R15–R24.